

IDENTIFICATION AND DISSECTION OF Ca²⁺-BINDING SITES IN THE
EXTRACELLULAR DOMAIN OF Ca²⁺-SENSING RECEPTOR*

Yun Huang^{1§}, Yubin Zhou^{1§}, Wei Yang¹, Robert Butters², Hsiau-Wei Lee¹, Shunyi Li¹, Adriana Castiblanco¹, Edward M. Brown², and Jenny J. Yang^{1†}

¹Department of Chemistry, Center for Drug Design and Advanced Biotechnology, Georgia State University, Atlanta, Georgia 30303

²Division of Endocrinology, Diabetes and Hypertension, Department of Medicine, Brigham and Women's Hospital, Boston, MA, 02115

Running title: Site-specific Ca²⁺ binding affinity in CaSR

Address correspondence to: Jenny J Yang, Department of Chemistry, Georgia State University, University Plaza, Atlanta, Georgia 30303 USA, Tel: 404-651-4620, Fax: 404-651-2751, Email: chejyy@langate.gsu.edu

Ca²⁺-sensing receptors (CaSRs) represent a class of receptors that respond to changes in the extracellular Ca²⁺ concentration ([Ca²⁺]_o) and activate multiple signaling pathways. A major barrier to advancing our understanding of the role of Ca²⁺ in regulating CaSRs is the lack of adequate information about their Ca²⁺-binding locations, which is largely hindered by the lack of a solved three dimensional structure and rapid off-rates owing to low Ca²⁺-binding affinities complicating direct binding studies. In this paper, we report the identification of three potential Ca²⁺-binding sites in a modeled CaSR structure using computational algorithms based on the geometric description and surface electrostatic potentials. Mutation of the predicted ligand residues in the full-length CaSR caused abnormal responses to [Ca²⁺]_o similar to those observed with naturally occurring activating or inactivating mutations of the CaR, supporting the essential role of these predicted Ca²⁺-binding sites in the sensing capability of the CaSR. In addition, to probe the intrinsic Ca²⁺ binding properties of the predicted sequences, we have engineered two predicted continuous Ca²⁺-binding sequences individually into a scaffold protein provided by a non-Ca²⁺-binding protein, CD2. We report herein the estimation of the metal-binding affinities of these predicted sites in the CaSR by monitoring aromatic-sensitized Tb³⁺ fluorescence energy transfer. Removing the predicted Ca²⁺-binding ligands resulted in the loss of or significantly weakened cation binding. The potential Ca²⁺-binding residues were shown to be involved in Ca²⁺/Ln³⁺ binding by high resolution NMR and site-

directed mutagenesis, further validating our prediction of Ca²⁺-binding sites within the extracellular domain of the CaSR.

Temporal and spatial changes of the Ca²⁺ concentration in the extra- and intracellular environments of cells affect the regulation of numerous cellular processes by modulating the activity of Ca²⁺-receptors and/or Ca²⁺-binding proteins (1-3). Multiple Ca²⁺-binding proteins with differing affinities have been identified in a variety of cellular compartments in all eukaryotic cells (4-6). Ca²⁺-binding proteins have Ca²⁺ affinities that vary by 10⁶-fold or more depending upon their locations and functions (7,8). Intracellularly, Ca²⁺-binding trigger proteins, such as calmodulin with its conserved EF-hand Ca²⁺-binding sites, have Ca²⁺-binding affinities in the submicromolar range (9). They respond to changes in the cytosolic free Ca²⁺ concentration ([Ca²⁺]_i) and regulate numerous cellular events and processes (10,11). Extracellularly, Ca²⁺ also functions as a first messenger to direct numerous intracellular functions (12-14). The Ca²⁺-sensing receptor (CaSR) that was initially cloned from the parathyroid gland (15) is a sensor of the extracellular Ca²⁺ concentration ([Ca²⁺]_o) that transforms the [Ca²⁺]_o stimulus into a variety of intracellular responses to regulate multiple signaling pathways, including activation of phospholipases C, A₂, and D, and inhibition of cAMP formation (16,17). This receptor, along with the metabotropic glutamate receptors (mGluR), γ -aminobutyric acid (GABA)_B receptors and receptors for pheromones, amino acids, and sweeteners, belongs to the family C of the G protein-coupled receptors (GPCR) superfamily. Most members in this family have

the capacity to sense $[Ca^{2+}]_o$ (18,19). More than one hundred mutations and polymorphisms have been identified in the CaSR that either inactivate (have a reduced sensitivity to $[Ca^{2+}]_o$) or activate (have an enhanced sensitivity to $[Ca^{2+}]_o$) the receptor, which cause familial hypocalciuric hypercalcemia (FHH) and neonatal severe hyperparathyroidism (NSHPT) in the former and autosomal dominant hypoparathyroidism (ADH) in the latter case (20,21).

The CaSR and other members of family C of the GPCR consist of a large extracellular domain (ECD), a transmembrane domain with seven transmembrane segments, and an intracellular C-tail segment (22,23). Based on the functional responses at the cellular level, the ECD regions have been proposed to contain the major Ca^{2+} -binding sites and to respond to $[Ca^{2+}]_o$ for both the mGluRs and CaSRs. The Hill coefficient suggests that 3-5 Ca^{2+} ions bind cooperatively to the CaSR (22,24). In addition to Ca^{2+} , the CaSR also responds to Mg^{2+} (25), polyamines, and amino-acids, such as L-Phe. Similar to the capacities of the mGluRs to respond to both L-Glu and high $[Ca^{2+}]_o$, the Ca^{2+} -induced activation of the CaSR is potentiated by L-amino acids, particularly aromatic amino acids (26).

Progress in understanding the mechanism mediating $[Ca^{2+}]_o$ regulation is largely hampered by a lack of knowledge regarding the Ca^{2+} -binding sites in the CaSR. To date, the identity of the Ca^{2+} -binding sites in the CaSR and related GPCRs still remains unknown. X-ray structural determination by Kunishima *et al.* revealed that the ECD of mGluR1 contain a Venus flytrap module (VFTM) (27). Key residues involved in glutamate binding were located at the interface between the two lobes (LB1 and LB2). However, no bound Ca^{2+} has been observed in these structures with or without the ligand glutamate (28). Major challenges in probing Ca^{2+} -binding sites in this class of receptors include the difficulties in crystallization, the rapid off rates owing to the low affinity of the Ca^{2+} binding and the existence of multiple conformations that are in equilibrium with one another (29). Indeed, successful crystallization of the CaSR ECD has not been reported despite a decade or more of effort directed to this end. Furthermore, methods for direct measurement of Ca^{2+} -binding to the CaSR have not yet been established (30,31) possibly due to its large size, multiple binding sites, and conformational flexibility.

To reveal the potential Ca^{2+} -sensing locations in the CaSR, in the paper, we first created model structures of the CaSR based on its structural homology to mGluR1. We then predicted several possible Ca^{2+} -binding sites using our established

computational algorithms based on the common structural properties of Ca^{2+} -binding sites in proteins. We have shown that removing the predicted ligand residues in the full-length CaSR results in significant changes in the intracellular responses to $[Ca^{2+}]_o$. Two predicted continuous Ca^{2+} -binding sites [e.g., sites with ligand binding sites within short continuous primary sequences (<30 residues)] were further validated by inserting the sequences individually into a non- Ca^{2+} -binding host protein, CD2. The resulting engineered proteins (designated CD2-CaSR1 and CD2-CaSR2) possess the ability to bind Ca^{2+} and Ln^{3+} , in which the predicted Ca^{2+} -binding residues were shown to be involved in Ca^{2+}/Ln^{3+} binding by high resolution NMR and site-directed mutagenesis, further validating our prediction of Ca^{2+} -binding sites within the ECD of the CaSR.

METHODS AND MATERIALS

Computational prediction of Ca^{2+} -binding sites from a model structure

A sequence alignment of the ECD region (1-540 residues) of the human CaSR and mouse mGluR has been carried out using the CLUSTALW program (32). Structural modeling of the CaSR has been performed using SWISS-MODEL (33,34) and the MODELLER (35) based on the structures of mGluR1 (pdb files 1EWT (27) and 1ISR (28)). Then the putative Ca^{2+} -binding sites in the CaSR were predicted using the program MetalFinder as described previously (36). Asp is used as the anchor ligand, because it is the most frequently used amino acid residue in Ca^{2+} -binding sites. The oxygen atoms from backbone carbonyls and the side-chains of Asp, Glu, Asn, Gln, Ser, Thr and Tyr were used as potential Ca^{2+} ligand residues. In the computational calculation, an increased Ca-O distance (1.0-4.0 Å) and O-Ca-O angles ($\pm 60^\circ$) were used to compensate for the uncertainties in the model structures (37-39). The resulting potential sites identified by the algorithm were scored and ranked based on the ligands. Those that use all native, existing residues of the CaSR sequence as the ligands receive the highest scores. The predicted sites that require mutations to similar residue types receive higher scores than others. Similar residue types refer to the following pairs: N-D, Q-E, D-E, and S-T. In contrast, the requirement of mutating non- Ca^{2+} -binding ligands suggests that the location does not bind Ca^{2+} in the native CaSR. Finally, the electrostatic potentials were calculated using the program DelPhi (40,41), and the model structures with the hydrogen atoms were built in by SYBYL. For the DelPhi

calculations, interior and exterior dielectric constants of 2 and 80, respectively, were used. The salt concentration was 0, and the linear solution of the Poisson Boltzmann equation was imposed until convergence was reached. The geometrically predicted locations with 2-4 negatively charged ligands, strong negative surface potential, and functionally necessary residues are more likely to bind Ca^{2+} . The model structures of CD2 variants with grafted potential Ca^{2+} -binding sites of the CaSR were generated by SWISSMODEL (33,34).

Measurement of $[\text{Ca}^{2+}]_i$ in cell population by fluorimetry

The $[\text{Ca}^{2+}]_i$ responses of wild type and mutant CaSRs was assessed as described by Bai et al. (42). In brief, the HEK293 cells transfected with the CaSR or its mutant cDNAs were loaded with fura-2/AM. The remaining extracellular fura-2/AM is washed out before the cells were transferred to a fluorescence cuvette. The emission at 510 nm was measured with excitation at 340 and 380 nm under varying $[\text{Ca}^{2+}]_o$ (0.5-20.5 mM). The ratio of the fluorescence intensities is used to derive $[\text{Ca}^{2+}]_i$. All measurements were carried out in triplicate. Data are expressed with the standard error of the mean (SEM) as the index of dispersion.

Protein engineering, expression and purification

The CaSR sequences G222-I235 (GIEKFREEAEERDI) and G383-I408 (GHEESGDRFSNSSTAFRPLCTGDENI) were individually inserted between S52 and G53 of CD2 in the plasmid pGEX-2T (denoted as CD2-CaSR1 and CD2-CaSR2, respectively) by PCR using an established protocol (63). Two mutants, CD2-CaSR1-E228A/E229A and CD2-CaSR2-E378A/E379A, were also made by site-directed mutagenesis. Three glycines at the N terminus and two at the C terminus of the inserted sequences were thereafter inserted using a similar procedure (denoted as CD2-CaSR1-5G and CD2-CaSR2-5G). The mutants of the engineered proteins were produced using standard PCR methods. All sequences were verified by automated sequencing on an ABI PRISM-377 DNA sequencer (Applied Biosystems) in the Advanced Biotechnology Core Facilities of Georgia State University.

The proteins were expressed as GST fusion protein using *Escherichia coli* BL21 (DE3) cells in LB medium with 100 mg/L of ampicillin at 37 °C. For ^{15}N isotopic labeling, $^{15}\text{NH}_4\text{Cl}$ was supplemented as the sole source of nitrogen in the minimal medium. 100 μM of isopropyl- β -D-thiogalactopyranoside (IPTG) was added when

the OD_{600} reaches 0.6 to induce protein expression for another 3 to 4 hours. The cells were collected by centrifuging at 5000 g for 30 min. The purification procedures followed the protocols for GST-fusion protein purification using glutathione sepharose 4B beads (GE Healthcare). The GST-tag of the proteins was cleaved on beads by thrombin. The eluted engineered CD2 variants were further purified using Superdex 75 and Hitrap SP columns (GE Healthcare). The purified proteins were confirmed by MALDI-TOF-MS in the Advanced Biotechnology Core Facilities of Georgia State University. The protein concentrations were determined using an ϵ_{280} of $11,700 \text{ M}^{-1} \text{ cm}^{-1}$ (43).

Electrospray Ionization Mass Spectrometry (ESI-MS)

The ESI-MS was performed using a Waters Micromass Q-TOF micro instrument. The data were acquired in positive ion mode by syringe pump infusion of the protein solutions at a flow rate of 7 $\mu\text{L}/\text{min}$. The protein sample stock (~1 mM) in 10 mM Tris, pH 7.4 was diluted 100-fold into water. Metal ions were added in 5-fold molar excess relative to the protein concentration.

Circular dichroism

The CD spectra were recorded from 190 to 260 nm on a Jasco-810 spectropolarimeter at ambient temperature using a quartz cell of 1 mm path length with protein concentrations ranging from 15 to 20 μM in 10 mM Tris-HCl, pH 7.4. All spectra were the average of ten scans with a scan rate of 100 nm/min. The spectra were converted to mean residue molar ellipticity after subtracting the spectrum of the buffer as the blank.

Fluorescence Spectroscopy

A PTI lifetime fluorimeter was used to record the fluorescence spectra at ambient temperature using a 1 cm path length cell. Intrinsic tryptophan emission spectra were recorded from 300 to 400 nm with the excitation wavelength at 282 nm. The slit widths were set at 4 and 8 nm for excitation and emission, respectively. Protein samples (1.5 to 3.0 μM) were in 20 mM PIPES-10 mM KCl at pH 6.8. For Tyr/Trp-sensitized Tb^{3+} fluorescence energy transfer (Tb^{3+} -FRET) experiments, emission spectra were collected from 500 to 600 nm with the excitation at 282 nm with slit widths for excitation and emission set at 8 and 12 nm, respectively. A glass filter with cutoff of 320 nm was used to circumvent secondary Rayleigh scattering. The Tb^{3+} titration was performed by gradually adding different

volumes of Tb³⁺ stock solutions (1 mM) into the protein samples (2.5 μM) in 20 mM PIPES, pH 6.8, with 10-150 mM KCl. For the Ca²⁺ competition studies, a solution containing 30 μM of Tb³⁺ and 1.5 μM of protein was set as the starting point. The stock solution of 10-100 mM CaCl₂ with the same concentration of Tb³⁺ and protein was gradually added in the initial mixture. The fluorescence intensity was normalized by subtracting the contribution of the baseline slope using logarithmic fitting. The Tb³⁺-binding affinity of protein was obtained by fitting normalized fluorescence intensity data using the equation

$$f = \frac{([P]_T + [M]_T + K_d) - \sqrt{([P]_T + [M]_T + K_d)^2 - 4[P]_T[M]_T}}{2[P]_T}$$

(Eq. 1)

where f is the fractional change, K_d is the dissociation constant for Tb³⁺, and $[P]_T$ and $[M]_T$ are the total concentrations of protein and Tb³⁺, respectively.

The Ca²⁺ competition data was firstly analyzed to derive the apparent dissociation constant by equation 1. By assuming that the sample is saturated with Tb³⁺ at the starting point of the competition, the Ca²⁺-binding affinity is further obtained by using the equation

$$K_{d,Ca} = K_{app} \times \frac{K_{d,Tb}}{K_{d,Tb} + [Tb]} \quad (\text{Eq. 2})$$

where $K_{d,Ca}$ and $K_{d,Tb}$ are the dissociation constants of Ca²⁺ and Tb³⁺, respectively. K_{app} is the apparent dissociation constant.

NMR spectroscopy

NMR spectra were collected on a 600 MHz NMR spectrometer. Two-dimensional TOCSY spectra were collected using a wgtocsy pulse sequence with an isotropic mixing time of 75 ms at 25 °C. The spectrum width was 13.3 ppm at both dimensions with a complex data point of 4096 at the first dimension and 400 increments at the second dimension. Two-dimensional (¹⁵N, ¹H)-HSQC NMR spectra were collected with 4096 complex data points at the ¹H dimension and 128 increments at the ¹⁵N dimension. Samples contained 1 mM of the protein in 20 mM PIPES-150 mM KCl, 10% D₂O at pH 6.8. All the NMR data were processed using FELIX (Accelrys) on a Silicon Graphics computer.

RESULTS

Prediction of Ca²⁺ binding sites in the CaSR

The ECD of the CaSR contains the majority of the Ca²⁺-sensing determinants, and glycosylation does not play a significant role in the activation of the receptor by high [Ca²⁺]_o. Both mGluR5

and CaSR respond to high [Ca²⁺]_o and are potentiated (activated) by L-amino acids (26). Their ECDs share ~30% sequence identity and a highly similar arrangement of secondary structural elements to that of mGluR. Therefore, we performed sequence alignment of the ECD region (1-540 residues) of the human CaSR and mouse mGluR, and then model structures of the ECD of the CaSR were created based on three structures of mGluR1: the ligand-free form (1EWT), the Glu- and Mg²⁺-bound forms (1EWK) (27), and the Glu- and Gd³⁺-bound form (1ISR) (28). Fig. 1 shows the model structure of the ECD of the CaSR with the Venus flytrap structure. Two subdomains, termed as Lobe 1 (N-terminus) and Lobe 2 (C-terminus), are linked by several loops. The structure is very similar to the model structures previously reported by Bai (22) and Silve et al. (44). This similarity of the models from different groups and methods strengthens the assumption that the model structures accurately represent the true structures of the CaSR.

We then predicted potential Ca²⁺-binding pockets in the modeled CaSR structure using our developed computational algorithms (Materials and Methods). Fig. 1 and Table 1 show three predicted potential Ca²⁺-binding pockets (Sites 1-3) in the modeled CaSR after the evaluation of their local geometric properties and electrostatic potentials. Site 1 is located in Lobe 2. It contains five glutamate residues in a 9-residue sequence (E224-E232). Three positive residues (K225, R227, and R233) and one aspartate residue (D234) are either in or follow this sequence closely. Site 2, located in Lobe 1, includes all of the predicted ligand residues in a 22-residue sequence (E378-E399), which are E378, E379, T396, D398, and E399. Predicted Sites 1 and 2 do not have extensive interactions with other parts of the protein. Site 3 is formed by residues S147, S170, D190, Y218, and E297, which are located in the crevice between the two lobes. All three sites are located at flexible loops or helical regions and are largely exposed on the surface of the protein. These geometrically predicted sites overlap with the negatively-charged "hot spots" predicted by the electrostatic potential (Fig. 1).

Effect of mutation of putative Ca²⁺ binding ligand residues on the biological function of the CaSR

The CaSR responds to elevated levels of [Ca²⁺]_o by activating phospholipase C, which leads to the production of IP₃ and further results in transient increases in the cytosolic Ca²⁺ concentration. To investigate the role of the proposed Ca²⁺-binding sites in the biological

function of the CaSR, we created several mutations in the predicted charged ligand residues in the full length CaSR. Specifically, we use site-directed mutagenesis to mutate the following residues: E297I in predicted site 3 located at the crevice, E224I and E228/229I in site CaSR-1 located in Lobe 2, and E378/379I and E398/399I in site CaSR2 located in lobe 1 (Tables 1-2). The wild type CaSR and the respective mutants were expressed in HEK293 cells using previously reported methods (45). The effects of the mutations on the biological function of the CaSR are summarized in Table 2 and Fig. 2. As shown in Fig. 2, removal of putative charged ligand residues at all three predicted Ca^{2+} -binding sites leads to significant alterations in either maximal Ca^{2+} response or/and sensitivity to $[\text{Ca}^{2+}]_o$ of the CaSR. E224I and the double mutant, E228/229I, at predicted site 1, decreases the maximal the Ca^{2+} responses by 35-38% with a slight left-shift in sensitivity to $[\text{Ca}^{2+}]_o$ ($\text{EC}_{50} = 2.5 \pm 0.3$ mM and 2.8 ± 0.2 mM, respectively vs. 3.1 ± 0.2 mM for the wild type CaSR, $n = 3$, $p < 0.05$). The mutation E398/399I in predicted site 2 also results in a 37% decrease in the maximal intracellular Ca^{2+} response. This mutant, however, exhibits a right-shifted EC_{50} of 4.4 ± 0.2 mM ($p < 0.01$). Interestingly, the E378/379I mutant at the same predicted site results in a 23% enhancement in the maximal response and a left-shifted EC_{50} ($\text{EC}_{50} = 2.2 \pm 0.1$ mM, $n = 3$, $p < 0.01$). Mutation E297I in Site 3 significantly impairs the sensitivity to the $[\text{Ca}^{2+}]_o$ response with an EC_{50} of 9.6 ± 0.2 mM.

Our functional characterization of the putative ligand residues in the predicted Ca^{2+} -binding sites of the CaSR are consistent with many mutations around the proposed Ca^{2+} -binding sites, which are associated with clinical syndromes (ADH and FHH) due to either a decrease or an increase in the sensitivity of the respective receptors to $[\text{Ca}^{2+}]_o$. By monitoring the intracellular Ca^{2+} response of HEK293 cells transfected with the wild type and mutant receptors, mutations of Ser147, Ser170, Asp190, Tyr218 and E297K were shown to largely impair the activation of the human CaSR (45-47). Recently, Silve *et al* have shown that the missense mutations, E297K and Y218S, significantly reduce the maximum Ca^{2+} -induced $[\text{H}^3]$ -IP response. They postulate that the residues S170, D190, Q193, S296 and E297 are critical for the CaSR's Ca^{2+} binding and downstream biological functions, which is in excellent agreement with our prediction. Although these findings are not based on direct measurement of Ca^{2+} binding, they provide

strong experimental evidence to support our model structures as well as the prediction of Ca^{2+} -binding sites in the ECD of the CaSR.

Engineering proteins by grafting the predicted sequences into CD2

Investigation of the site-specific Ca^{2+} -binding properties of the CaSR is one important step toward fully understanding the mechanism underlying its Ca^{2+} -modulated functions. Our lab has previously established a grafting approach to investigate the site-specific metal-binding properties of CaM by inserting the individual EF-loops of CaM into a host frame, CD2 (48). Since predicted Ca^{2+} -binding sites 1 and 2 of the CaSR have contiguous stretches of amino acids, similar to the Ca^{2+} -binding motifs in CaM, we extended the grafting approach to probe the site-specific Ca^{2+} -binding affinity of these two sites. The continuous sequences were inserted into CD2 at position 52 between the strands C' and D, since our previous studies have shown that this position tolerates the insertion of EF-hand motifs from CaM. The distances between the two termini of the inserted Ca^{2+} -binding sites in the model structures of the CaSR are within 15 Å. Accordingly, a total of 5-6 glycine linkers is sufficient to enable the grafted motifs to retain a native metal-binding conformation (48), and two more variants were thus engineered with 3 and 2 flanking Gly residues at the N- and C-termini of the CaSR sequence. Fig. 3 shows the modeled structure of CD2 with grafted Ca^{2+} -binding sites from the CaSR. Trp32 and Tyr76 in the host proteins are about 12 Å distant from the grafted sites, which enables aromatic-sensitized energy transfer to the Tb^{3+} bound to the sites, providing a spectroscopic method to monitor the metal-binding process.

The conformation of scaffold protein is not altered after grafting Ca^{2+} -binding sites

To ensure that the grafted Ca^{2+} -binding site has no major interaction with the host protein, and that the host protein has not changed its native conformation, we carried out conformational analyses using various methods. As shown in Fig. 4A, the far UV CD spectra of all four engineered proteins showed a trough at 216 nm, indicating a typical β -sheet secondary structure, as in the wild type CD2. The deeper negative molar ellipticity in the short-wavelength region compared to that of CD2 is consistent with the addition of loop/less structured sequences of the CaSR. In addition, the Trp fluorescence spectrum of wild type CD2 overlaps that of the engineered proteins, both of which exhibit two peaks at 314 and 335 nm, suggesting that the Trp

environment remains unchanged after engineering of the protein (Fig. 4B). Furthermore, the majority of the NMR chemical shifts of the host frame in the engineered variants were not significantly different from those of CD2 (Fig. 4C), suggesting that the scaffold protein was minimally perturbed after the insertion of the foreign sequences. All of these results implied that the host scaffold protein retained its native structure, thereby ensuring a minimal contribution to the metal-binding of the inserted sequences.

The grafted sequences from CaSR bind cations

The Ca^{2+} -binding capability of the inserted sequences was first revealed by NMR. Upon the addition of 10 mM Ca^{2+} under high salt conditions (150 mM KCl), several residues from the inserted sequences have altered resonances as shown in the HSQC spectra (Fig. 5). For example, Ca^{2+} binding resulted in chemical shift changes of at least two of the peaks arising from glutamates in CD2-CaSR1-5G (Fig. 5A). The addition of Mn^{2+} led to the disappearance of resonances from the inserted sequences and the CD2 host residues in proximity, due to the line-broadening effect caused by the Mn^{2+} that substitutes for the Ca^{2+} (data not shown). In contrast, wild type CD2 does not exhibit any detectable changes under identical conditions. Furthermore, the addition of La^{3+} to the CD2-CaSR2 led to significant changes of, for example, at least two resonances originating from the grafted sequence as well as Gly53 of CD2 (Fig. 5C). More convincingly, after substituting two proposed Ca^{2+} -binding ligand residues within Site 1 (E228/229) or Site 2 (E378/E379) with alanines, we could not detect such significant chemical shift changes upon addition of metal ions (Figs. 5B and D), further supporting the involvement of these residues in the chelation of Ca^{2+} within each predicted metal-binding site. Mutagenesis studies on these putative Ca^{2+} -binding ligands have also been shown to affect the biological function of CaSR (Fig. 2). Moreover, the mass peaks corresponding to the formation of 1:1 Ca^{2+} -protein or Tb^{3+} -protein complexes were observed in ESI-MS spectra in the presence of excess metal ions (Fig. 6). These results suggest that the inserted sequences from the CaSR have the capacity to bind Ca^{2+} and its trivalent analogs.

The addition of Tb^{3+} into the engineered proteins (Fig. 7A) or *vice versa* resulted in large increases of Tb^{3+} fluorescence at 545 nm due to Trp-sensitized Tb^{3+} -fluorescent resonance energy transfer (Tb^{3+} -FRET) (36,49), which was not observed for wild type CD2. The addition of

Ca^{2+} into the Tb^{3+} -protein mixture decreases the Tb^{3+} signal due to competition (Fig. 7B). The Tb^{3+} - and Ca^{2+} -binding affinities were derived from the Tb^{3+} fluorescence change and the metal competition, respectively. For CD2-CaSR1, the Tb^{3+} - and Ca^{2+} -binding dissociation constants obtained were 35 ± 3 and 890 ± 80 μM at low salt concentrations, respectively. At high salt concentrations (e.g., ~ 150 mM NaCl) as in the extracellular environment within which the extracellular domain of the native CaSR normally resides, the Ca^{2+} -binding affinity decreased at least 10-fold (Table 3). For CD2-CaSR2, the Tb^{3+} and Ca^{2+} dissociation constants were 25 ± 2 μM and 4.3 ± 0.8 mM at low and 98 ± 7 μM and 18.6 ± 0.5 mM at high salt concentrations, respectively. The relatively stronger affinity for Tb^{3+} than for Ca^{2+} is consistent with other natural Ca^{2+} -binding proteins and is partly due to the electrostatic nature of the metal binding (50). Further, the variants with or without flanking glycine linkers exhibit no significant differences in their metal-binding affinities, suggesting that the grafted Ca^{2+} -binding sites are flexible and less sensitive to the host protein.

Site-directed mutagenesis that removed the predicted charged ligand residues resulted in a dramatic decrease of the Tb^{3+} -FRET signal, suggesting attenuated metal binding affinities. For example, the Tb^{3+} fluorescence enhancements of both mutants E378/379A and D398/E399A are 70% lower than that of CD2-CaSR2. The signal of the mutant E231/232A is also 30% lower than that of CD2-CaSR. These results are consistent with our functional study of the mutations (Fig. 2 and Table 2) and further validate our prediction of Ca^{2+} binding sites in the ECD of the CaSR.

DISCUSSION

Predicting Ca^{2+} -binding in the CaSR and the effect of mutations on the function of the CaSR

Ca^{2+} bound to proteins is predominantly chelated with oxygens with an average coordination of 6-7 (51-53). The binding of Ca^{2+} to multiple sites in a highly cooperative manner facilitates the response of a protein to small Ca^{2+} concentration changes (54-56), such as the binding of four Ca^{2+} ions to CaM. The Hill coefficient suggests that 3-5 Ca^{2+} ions bind cooperatively to the CaSR. However, the Ca^{2+} -binding sites have not been identified.

Our laboratory has shown that naturally-evolved Ca^{2+} -binding sites can be identified and novel Ca^{2+} -binding proteins can be designed using the

pentagonal bipyramidal geometry with the side-chains of the aforementioned residues and main-chain carbonyls as potential ligands (53). In this study, taking advantage of the previously determined structures of mGluR1 and the sequence homology of the CaSR to mGluR1, we predicted several Ca^{2+} -binding sites in the modeled structure of the CaSR by applying our well-developed computational algorithms. These sites possess high electrostatic potential and are located in the negatively charged environments (Fig. 1), which are preferred for Ca^{2+} binding (36). In addition, these putative Ca^{2+} binding sites are located in the flexible locations either in the crevices between two lobes (site 3) and/or at loop and exposed regions. This is consistent with a survey that revealed that almost all of the known Ca^{2+} -binding sites are located in or adjacent to the flexible structures of their respective proteins, such as loop regions, turns, or the ends of α -helices and β -sheets (57).

Our model structure and predicted Ca^{2+} -binding sites, especially Site 3, are consistent with the reported functional studies. The X-ray structure of mGluR1 complexed with its ligand, glutamate, reveals that the residues S164, S165, T188, Y236, and E292 in the protein form hydrogen bonds with the α -carboxyl group of the glutamate (58). These residues correspond to S147, S170, D190, Y218 and E297 in the CaSR, respectively. Two mutations, Y218S and E297K, markedly reduce the responsiveness and sensitivity of the receptor to $[\text{Ca}^{2+}]_o$ (24). Furthermore, mutations around these predicted locations have been shown to alter the Ca^{2+} response of cells expressing the respective mutant receptors, supporting our prediction. For example, T151M in ADH and R185Q in FHH are adjacent to Ca^{2+} ligand residues in Site 3. Additional mutations that alter the CaSR responses, such as Y218S/C, E297K, and R220S and R221S, are also either at or near the predicted ligand residues of Site 3 (59,60). In addition, Zhang *et al.* have demonstrated that S170 is critical for functional modulation of the CaSR by L-Phe, in that the S170A mutation led to no significant change in the EC_{50} of the protein for $[\text{Ca}^{2+}]_o$ but a 1.6-fold increase in its response at 50 mM $[\text{Ca}^{2+}]_o$ (24). Recently, Mun *et al.* further showed that the double mutation, T145A/S170T, selectively disables L-amino acid sensing but does not change the $[\text{Ca}^{2+}]_o$ -sensing capability of the CaSR (61), thereby suggesting that the two processes can be dissociated and that the L- amino acid is mainly bound near S170.

The predicted Ca^{2+} -binding site in the crevice is likely to play a central role in modulating the

function of the CaSR by Ca^{2+} -induced conformational changes. Previous studies have shown that mutations in this site inactivate the protein (44). The mutations, E297I and D215I, provide additional support for this hypothesis. The glutamate-binding site in mGluR is also within the crevice of the protein, suggesting that the hinge that connects the two lobes directly responds to the stimuli inducing receptor activation in the GPCR family C proteins.

The mutations outside of the crevice demonstrate the complexity of the regulatory mechanism of the CaSR. Removal of charged residues in both Lobe 1 (E224I and E228/229I) and Lobe 2 (E398/399I) decreases the maximal response levels but results in oppositely directed changes in the sensitivity of the receptor to $[\text{Ca}^{2+}]_o$. Perhaps the maximal responses and the sensitivity are determined by different locations of the protein via distinct mechanisms. In addition, loss of the charges on these residues might alter the interactions of these amino acids with charged residues elsewhere on the protein, potentially favoring conformations that either activate or inactivate the protein, depending on local geometrical factors. Since both mutations result in significantly weakened metal-binding in the CD2-CaSR variants, the results suggest that Ca^{2+} binding at the predicted locations are necessary for maintaining the full function of the CaSR. Therefore, Ca^{2+} acts as both a stimulus and a regulator for the CaSR. The potential Ca^{2+} binding to E398/399 might be crucial since removal of these two charges causes a dual effect by decreasing both the maximal activity and the sensitivity to $[\text{Ca}^{2+}]_o$.

Grafting approach for probing Ca^{2+} binding capability

To overcome the limitations of solely investigating the Ca^{2+} -binding sites in native proteins, we have established a grafting approach to dissect their site specific properties. This approach has been used in the investigation of single EF-hand motifs in CaM (62,63). CD2 has been shown to be a suitable host system, since it retains its native structure after insertion of the foreign sequences, both in the presence and absence of Ca^{2+} ions, so that the influence of the host protein on the inserted sites is minimized. The difficulties inherent in directly confirming the predicted Ca^{2+} -binding ligands due to the multiple binding and conformational changes of the CaSR prompted us to investigate this issue indirectly using the grafting approach. In CD2-CaSR variants, additional residues and glycine linkers are at both termini of the predicted sequences to provide the

conformational freedom needed for the formation of their native structures. In addition, the host protein retains the native structure of CD2, as indicated by CD, fluorescence, and NMR studies with and without cations. The addition of cations induced chemical shift changes of the resonances arising from the inserted sequences but not those from the host proteins, indicating that the binding is independent of the host protein and occurs at the inserted sequences.

The capability of the two predicted Ca^{2+} -binding sites of the CaSR grafted into CD2 to bind Ca^{2+} and Ln^{3+} validated our computational identifications. In the CaSR model structures, the predicted sequences are in flexible loop regions. In CD2-CaSR variants, these sequences are also in flexible loops indicated by the far-UV CD spectra. The variants with or without glycine linkers exhibit similar Tb^{3+} and Ca^{2+} binding affinities, which also implies that these Ca^{2+} -binding sites are highly flexible, and the contribution of the host protein frame to the metal binding is less likely to be significant. The probed site-specific Ca^{2+} -binding affinities at 150 mM NaCl for CD2-CaSR1 and CD2-CaSR2 are 4.2 ± 0.3 and 18.6 ± 0.5 mM, respectively. These affinities are weaker than the EC_{50} of the CaSR (Table 2-3), which can be explained by several possible factors. First, the interaction of coupled metal-binding sites and cooperativity are likely to contribute to the overall sensing capacity of the intact CaSR to respond to $[\text{Ca}^{2+}]_o$. This is similar to the contribution of the cooperativity observed for CaM. This cooperativity could be the result of direct site-to-site interactions or through Ca^{2+} -induced conformational change. The cooperativity is not necessarily positive in all cases. In fact, the opposite effects of the mutations at predicted sites 1 and 2 on the sensitivity of the protein to $[\text{Ca}^{2+}]_o$ indicate that Ca^{2+} binding at various locations within the CaR ECD has diverse influences on the subsequent Ca^{2+} binding to other sites. If calcium effectively cross-linked and neutralized negative charges in two different parts of the molecule (one of which was one of our binding sites), for example, which then caused the lobes to close, then loss of one of those negative charges could reduce the repulsion between the negative charges that was present in the absence of calcium and favor activation of the receptor at lower extracellular calcium. Second, other factors, such as dimer

formation and the protein environment (e.g. hydrogen bonding and salt bridges), may also play a part in the affinity differences between the isolated sites and the full protein. In the engineered proteins, the host protein has minimal effects on metal binding. However, in the native CaSR, the surrounding residues will surely influence the electrostatic potentials at the Ca^{2+} -binding sites, in a Ca^{2+} -dependent or -independent manner. Third, it is possible that there are additional Ca^{2+} ligands for the sites that have not been identified in our prediction. Our work has opened up the opportunity for investigating the mechanism(s) underlying Ca^{2+} -modulated function by determining Ca^{2+} -binding properties in CaSRs at local levels.

In conclusion, several Ca^{2+} -binding sites have been predicted in the model structure of the CaSR. Two continuous predicted sites have been grafted into the host protein CD2. The metal binding studies on the engineered proteins using various spectroscopic methods validate the computational predictions and demonstrate the Ca^{2+} -binding capability of the predicted sequences. Mutations that remove the predicted charged Ca^{2+} ligand residues lead to weakened metal binding in the engineered proteins and abnormal responses to $[\text{Ca}^{2+}]_o$ in the full length CaSR, supporting the predictions and indicating the importance of Ca^{2+} -binding in regulating CaSR functions.

ACKNOWLEDGMENTS

We thank Dr. April L. Ellis for the experimental procedures and techniques used in the study, Dr. Lisa Jones for the electrostatic calculation and Julian Johnson and Michael Kirberger for helpful suggestions. We thank Drs. Jun-tao Guo and Youxing Qu at UGA for their generous help in structural modeling. We thank other members in JJY's laboratory for helpful discussions. This work was supported in part by the following sponsors: NIH GM070555, NIH GM 62999 and NSF MCB-0092486, AHA Foundation grant 0655168B to JJY and a Predoctoral Fellowship from the Brain and Behavior Program at Georgia State University to YH. EMB acknowledges support from NIH grants, DK52005 and DK67155.

FOOTNOTES

§These authors made equal contributions to this work and should both be considered as first authors.

*This work was supported in part by grants NIH GM 62999-1 and AHA 0655168B to JJY.

† To whom correspondence should be addressed. Tel: 404-651-4620; Email: chejyy@langate.gsu.edu.

REFERENCE

1. Carafoli, E. (2002) *Proc Natl Acad Sci U S A* **99**(3), 1115-1122
2. Berridge, M. J., Bootman, M. D., and Lipp, P. (1998) *Nature* **395**(6703), 645-648
3. Maurer, P., Hohenester, E., and Engel, J. (1996) *Curr Opin Cell Biol* **8**(5), 609-617
4. Michalak, M., Robert Parker, J. M., and Opas, M. (2002) *Cell Calcium* **32**(5-6), 269-278
5. Ikura, M., Osawa, M., and Ames, J. B. (2002) *Bioessays* **24**(7), 625-636
6. Feske, S., Okamura, H., Hogan, P. G., and Rao, A. (2003) *Biochem Biophys Res Commun* **311**(4), 1117-1132
7. Goll, D. E., Thompson, V. F., Li, H., Wei, W., and Cong, J. (2003) *Physiol Rev* **83**(3), 731-801
8. Teplyakov, A. V., Kuranova, I. P., Harutyunyan, E. H., Vainshtein, B. K., Frommel, C., Hohne, W. E., and Wilson, K. S. (1990) *J Mol Biol* **214**(1), 261-279.
9. Kawasaki, H., Nakayama, S., and Kretsinger, R. H. (1998) *Biometals* **11**(4), 277-295
10. Ermak, G., Morgan, T. E., and Davies, K. J. (2001) *J Biol Chem* **276**(42), 38787-38794
11. Zhang, X., and Joseph, S. K. (2001) *Biochem J* **360**(Pt 2), 395-400
12. Breitwieser, G. E., Miedlich, S. U., and Zhang, M. (2004) *Cell Calcium* **35**(3), 209-216
13. Handford, P. A. (2000) *Biochim Biophys Acta* **1498**(2-3), 84-90
14. Maki, M., Kitaura, Y., Satoh, H., Ohkouchi, S., and Shibata, H. (2002) *Biochim Biophys Acta* **1600**(1-2), 51-60
15. Brown, E. M., Gamba, G., Riccardi, D., Lombardi, M., Butters, R., Kifer, O., Sun, A., Hediger, M. A., Lytton, J., and Hebert, S. C. (1993) *Nature* **366**(6455), 575-580
16. Brown, E. M., and MacLeod, R. J. (2001) *Physiol Rev* **81**(1), 239-297
17. Bai, M. (1999) *Int J Mol Med* **4**(2), 115-125
18. Jingami, H., Nakanishi, S., and Morikawa, K. (2003) *Curr Opin Neurobiol* **13**(3), 271-278
19. Zonta, M., Sebelin, A., Gobbo, S., Fellin, T., Pozzan, T., and Carmignoto, G. (2003) *J Physiol* **553**(Pt 2), 407-414
20. Hu, J., Mora, S., Weber, G., Zamproni, I., Proverbio, M. C., and Spiegel, A. M. (2004) *J Bone Miner Res* **19**(4), 578-586
21. Sayer, J. A., and Pearce, S. H. (2003) *Clin Endocrinol (Oxf)* **59**(4), 419-421
22. Bai, M. (2004) *Cell Calcium* **35**(3), 197-207
23. Quinn, S. J., Bai, M., and Brown, E. M. (2004) *J Biol Chem* **279**(36), 37241-37249
24. Zhang, Z., Sun, S., Quinn, S. J., Brown, E. M., and Bai, M. (2001) *J Biol Chem* **276**(7), 5316-5322
25. Vetter, T., and Lohse, M. J. (2002) *Curr Opin Nephrol Hypertens* **11**(4), 403-410
26. Francesconi, A., and Duvoisin, R. M. (2004) *J Neurosci Res* **75**(4), 472-479
27. Kunishima, N., Shimada, Y., Tsuji, Y., Sato, T., Yamamoto, M., Kumasaka, T., Nakanishi, S., Jingami, H., and Morikawa, K. (2000) *Nature* **407**(6807), 971-977
28. Tsuchiya, D., Kunishima, N., Kamiya, N., Jingami, H., and Morikawa, K. (2002) *Proc Natl Acad Sci U S A* **99**(5), 2660-2665
29. Yang, W., Wilkins, A. L., Li, S., Ye, Y., and Yang, J. J. (2005) *Biochemistry* **44**(23), 8267-8273
30. Nagar, B., Overduin, M., Ikura, M., and Rini, J. M. (1996) *Nature* **380**(6572), 360-364
31. Hu, J., and Spiegel, A. M. (2003) *Trends Endocrinol Metab* **14**(6), 282-288
32. Higgins, D. G. (1994) *Methods Mol Biol* **25**, 307-318
33. Kopp, J., and Schwede, T. (2004) *Pharmacogenomics* **5**(4), 405-416
34. Schwede, T., Kopp, J., Guex, N., and Peitsch, M. C. (2003) *Nucleic Acids Res* **31**(13), 3381-3385
35. Marti-Renom, M. A., Stuart, A. C., Fiser, A., Sanchez, R., Melo, F., and Sali, A. (2000) *Annu*

- Rev Biophys Biomol Struct* **29**, 291-325
36. Yang, W., Wilkins, A. L., Ye, Y., Liu, Z. R., Li, S. Y., Urbauer, J. L., Hellinga, H. W., Kearney, A., van der Merwe, P. A., and Yang, J. J. (2005) *J Am Chem Soc* **127**(7), 2085-2093
 37. Hellinga, H. W., and Richards, F. M. (1991) *J Mol Biol* **222**(3), 763-785.
 38. Yang, W., Jones, L. M., Isley, L., Ye, Y., Lee, H. W., Wilkins, A., Liu, Z. R., Hellinga, H. W., Malchow, R., Ghazi, M., and Yang, J. J. (2003) *J Am Chem Soc* **125**(20), 6165-6171
 39. Deng, H., Chen, G., Yang, W., and Yang, J. J. (2006) *Proteins* **64**(1), 34-42
 40. Honig, B., and Nicholls, A. (1995) *Science* **268**(5214), 1144-1149
 41. Nicholls, A., and Honig, B. (1991) *J Comput Chem* **12**, 435-445
 42. Bai, M., Quinn, S., Trivedi, S., Kifor, O., Pearce, S. H., Pollak, M. R., Krapcho, K., Hebert, S. C., and Brown, E. M. (1996) *J Biol Chem* **271**(32), 19537-19545
 43. Driscoll, P. C., Cyster, J. G., Somoza, C., Crawford, D. A., Howe, P., Harvey, T. S., Kieffer, B., Campbell, I. D., and Williams, A. F. (1993) *Biochem Soc Trans* **21**(4), 947-952
 44. Silve, C., Petrel, C., Leroy, C., Bruel, H., Mallet, E., Rognan, D., and Ruat, M. (2005) *J Biol Chem* **280**(45), 37917-37923
 45. Zhang, Z., Qiu, W., Quinn, S. J., Conigrave, A. D., Brown, E. M., and Bai, M. (2002) *J Biol Chem* **277**(37), 33727-33735
 46. Tu, C. L., Oda, Y., Komuves, L., and Bikle, D. D. (2004) *Cell Calcium* **35**(3), 265-273
 47. Chang, W., and Shoback, D. (2004) *Cell Calcium* **35**(3), 183-196
 48. Ye, Y., Lee, H. W., Yang, W., and Yang, J. J. (2005) *J Inorg Biochem* **99**(6), 1376-1383
 49. Ye, Y., Shealy, S., Lee, H. W., Torshin, I., Harrison, R., and Yang, J. J. (2003) *Protein Eng* **16**(6), 429-434
 50. Falke, J. J., Drake, S. K., Hazard, A. L., and Peersen, O. B. (1994) *Q Rev Biophys* **27**(3), 219-290
 51. Glusker, J. P. (1991) *Adv Protein Chem* **42**, 1-76
 52. Dudev, T., Chang, L. Y., and Lim, C. (2005) *J Am Chem Soc* **127**(11), 4091-4103
 53. Yang, W., Lee, H. W., Hellinga, H., and Yang, J. J. (2002) *Proteins* **47**(3), 344-356.
 54. Akke, M., Forsen, S., and Chazin, W. J. (1995) *J Mol Biol* **252**(1), 102-121
 55. Hiraoki, T., and Vogel, H. J. (1987) *J Cardiovasc Pharmacol* **10 Suppl 1**, S14-31
 56. Malmberg, N. J., Varma, S., Jakobsson, E., and Falke, J. J. (2004) *Biochemistry* **43**(51), 16320-16328
 57. Pidcock, E., and Moore, G. R. (2001) *J Biol Inorg Chem* **6**(5-6), 479-489
 58. Suzuki, Y., Moriyoshi, E., Tsuchiya, D., and Jingami, H. (2004) *J Biol Chem* **279**(34), 35526-35534
 59. Pearce, S. H., Trump, D., Wooding, C., Besser, G. M., Chew, S. L., Grant, D. B., Heath, D. A., Hughes, I. A., Paterson, C. R., Whyte, M. P., and et al. (1995) *J Clin Invest* **96**(6), 2683-2692
 60. Cetani, F., Pardi, E., Borsari, S., Tonacchera, M., Morabito, E., Pinchera, A., Marcocci, C., and Dipollina, G. (2003) *Clin Endocrinol (Oxf)* **58**(2), 199-206
 61. Mun, H. C., Franks, A. H., Culverston, E., Krapcho, K., Nemeth, E. F., and Conigrave, A. D. (2004) *J Biol Chem*
 62. Sorensen, B. R., Faga, L. A., Hultman, R., and Shea, M. A. (2002) *Biochemistry* **41**(1), 15-20.
 63. Ye, Y., Lee, H. W., Yang, W., Shealy, S. J., Wilkins, A. L., Liu, Z. R., Torshin, I., Harrison, R., Wohlhueter, R., and Yang, J. J. (2001) *Protein Eng* **14**(12), 1001-1013

FIGURE LEGENDS

FIG 1. (A) **Model structure of the Ca²⁺-sensing receptor based on the X-ray structure of the ECD domain of mGluR1** (pdb code: 1EWT), which contains a Venus flytrap motif that is conserved in more than 11 different proteins, including the bacterial periplasmic binding proteins, maltose-binding proteins, and galactose-binding proteins. Two subdomains are connected by a flexible hinge region. Like other small molecules, such as maltose and galactose, Glu binds to the hinge region, resulting in a large conformational change with a hinge movement. (B) **Electrostatic surface analysis on the model structure of the ECD of the CaSR**. Circled positions are the predicted Ca²⁺-binding sites, which are rich in negatively charged residues. (C) **Model structure of Ca²⁺-binding sites of Sites 1-3**. Proposed Ca²⁺-binding ligand residues are labeled.

FIG. 2. **Effect of mutations in charged residues of the predicted Ca²⁺-binding sites on the responsiveness of the CaSR by monitoring intracellular Ca²⁺ using Fura-2**. Functional characterization of the wt CaSRs and CaSRs with mutations in Site 1 (A), Site 2 (B) or Site 3 (C) were performed using HEK293 cells transfected with the wt and CaSR mutated in charged residues and are expressed as the normalized Ca²⁺ responses.

FIG.3. **Modeled structure of CD2 with grafted Ca²⁺-binding sites in the CaSR**. Trp 32 and Y76 in the host protein are about 12 Å away from the grafted Ca²⁺-binding sites.

FIG. 4. **The secondary structures of wt CD2 and engineered proteins**. (A) Far UV CD spectra of 15 μM of wt CD2, CD2-CaSR1, CD2-CaSR1-5G, CD2-CaSR2 and CD2-CaSR2-5G in 10 mM Tris, pH 7.4. (B) Trp fluorescence spectra of wild type CD2 and the engineered proteins with grafted Ca²⁺-binding sites. (C) Comparison of chemical shifts of the alpha and backbone amide protons between wild type CD2 and the engineered protein CD2-CaSR1 with grafted Ca²⁺-binding sites from the CaSR.

FIG. 5. **{¹H, ¹⁵N}-HSQC spectra of CD2-CaSR1, CD2-CaSR2 and their mutants**. (A) Ca²⁺-induced chemical shift changes of two peaks arising from the 4 glutamates in the grafted Ca²⁺-binding sequence in CD2-CaSR1. This result provides direct evidence of Ca²⁺-induced movement of residues (Glu) within the grafted Ca²⁺-binding motif. Blue: CD2-CaSR1 with 1 mM EGTA; Red: CD2-CaSR1 with 10mM Ca²⁺. (B) Superimposed HSQC spectrum of CD2-CaSR1-E228A/229A in the presence of 0.1 mM EGTA (blue) or 10 mM Ca²⁺ (red). No significant chemical shift changes were observed for the resonances from the inserted sequences (boxes). (C) La³⁺-induced chemical shift changes of one of the linker residues, glycine 53 (left), and two resonances from the grafted CaSR2 sequence (right, boxed region). Meanwhile, the chemical shifts of resonances from the host framework (I14, N20, D25, G35, E41, R70, S82, and T83) remained almost unaltered. Blue: CD2-CaSR2 with 1 mM EGTA; Red: CD2-CaSR2 with 1mM La³⁺. (D) Overlaid HSQC spectrum of CD2-CaSR2-E378A/379A in the presence of 0.1 mM EGTA (blue) or 1 mM La³⁺ (red). The addition of La³⁺ did not lead to chemical shift changes of glycine 53 or peaks originating from the inserted sequences (dashed boxes). The insert is another enlarged region of HSQC spectrum. The new resonance (dashed circle) emerged after mutagenesis was from one of the alanine residues in the inserted sequence. Addition of La³⁺ did not cause significant chemical shift change.

FIG. 6. **ESI-MS spectra of CD2-CaSR1 with metal ions**. The binding of Ca²⁺ or Tb³⁺ led to the emergence of additional peaks with molecular mass differences of +38 and +146, respectively.

FIG. 7. **Probing metal-binding with aromatic residue-sensitized Tb³⁺-FRET**. (A) The enhancement of Tb³⁺ fluorescence of CD2-CaSR1 at 545 nm as a function of titrated Tb³⁺. A 1:1 binding mode was assumed for data fitting. (B) Ca²⁺ competition assay. The addition of Ca²⁺ led to a decrease of Tb³⁺ fluorescence due to competitive binding of metal ions in CD2-CaSR1 that was preincubated with Tb³⁺. (C) Comparison of relative Tb³⁺ signal changes of w.t. CD2-CaSR2 and its charged mutants.

TABLE 1
Predicted Ca²⁺ binding sites and their corresponding mutations in diseases

Predicted sites	Residues	Disease Related Mutations	
		Site Mutations	Environmental Mutations
Site 1	E224, E228, E229, E231, E232	<i>NSPHT</i> : D215G <i>ADH</i> : E228Q	<i>NSPHT</i> : Y218G/S, R220W/Q, P221S, R227L/Q, E250K <i>ADH</i> : P221L, Q245R
Site 2	E378, E379, T396, D398, E399	N/A	<i>FHH/NSPHT</i> : C395R
Site 3	S147, S170, D190, Y218, E297	<i>FHH/NSPHT</i> : S147A, S170A, D190K, Y218S, E297K	<i>FHH/NSPHT</i> : S137P, T138M, E191K, D215G, R220W/Q, P221S <i>ADH</i> : T151M

TABLE 2
Summary of the maximal response and EC₅₀ values of CaSR and its mutants

Predicted site	Mutation	Maximal response (%)	Ca ²⁺ , EC ₅₀ (mM)
	WT	100	3.1 ± 0.2
Site 1	E224I	65 ± 1**	2.5 ± 0.3*
	E228/229I	62 ± 6**	2.8 ± 0.2
Site 2	E378/379I	123 ± 6*	2.2 ± 0.1**
	E398/399I	63 ± 12*	4.4 ± 0.2**
Site 3	E297I	87 ± 6	9.6 ± 0.2**

** : p<0.01; * : p<0.05

TABLE 3
Dissociation constants of CD2 variants with grafted Ca²⁺-binding sequences from the CaSR

	Tb ³⁺ (μM)		Ca ²⁺ (μM)	
	10 mM KCl	150 mM NaCl	10 mM KCl	150 mM NaCl
CD2-CaSR1	35 ± 3	144 ± 5	890 ± 80	4200 ± 400
CD2-CaSR1-5G	7 ± 1	94 ± 7	400 ± 240	5000 ± 700
CD2-CaSR2	25 ± 2	98 ± 7	4300 ± 800	18600 ± 500
CD2-CaSR2-5G	19 ± 2	80 ± 3	2400 ± 1000	6100 ± 200

Figure 1

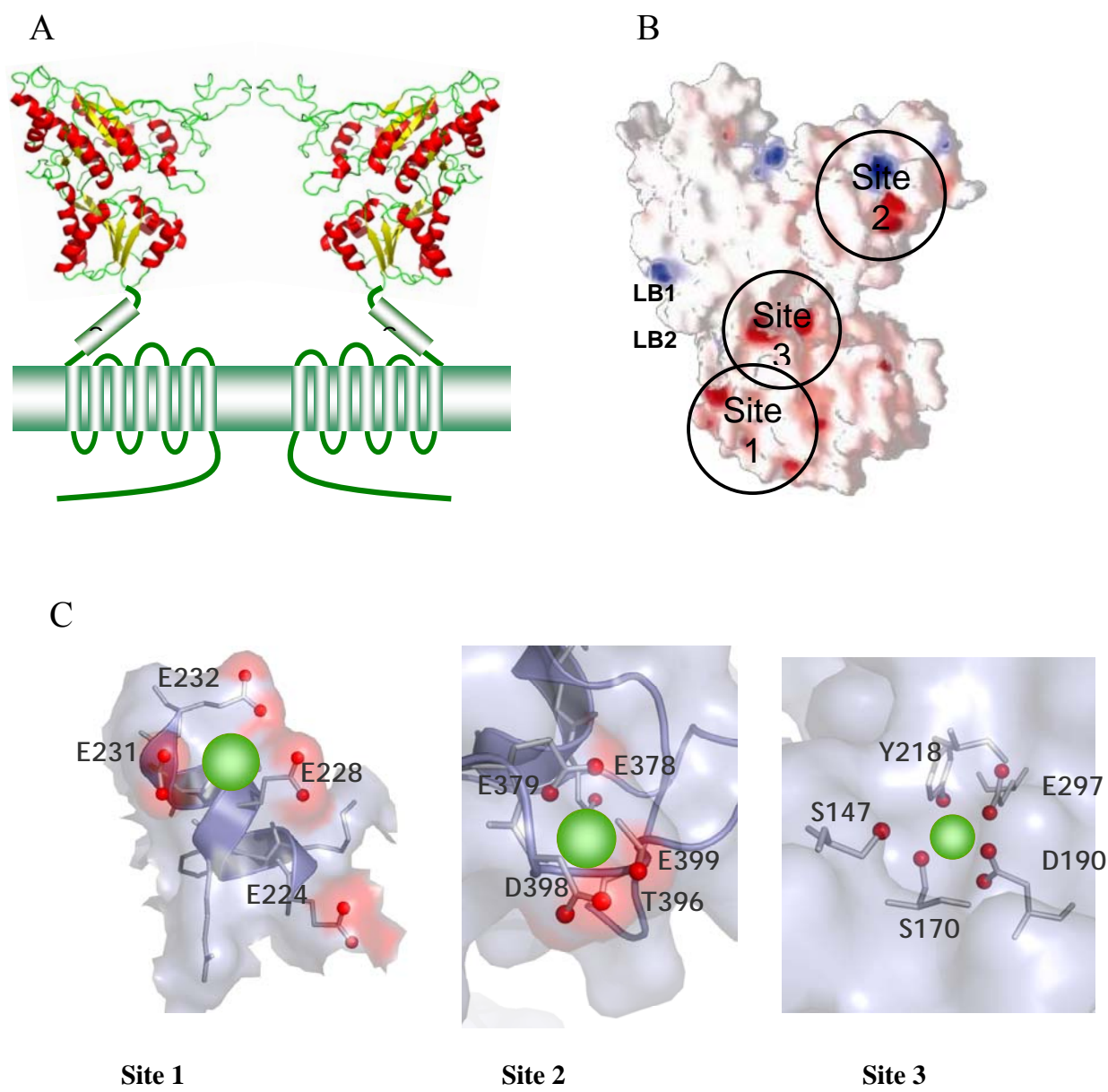


Figure 2

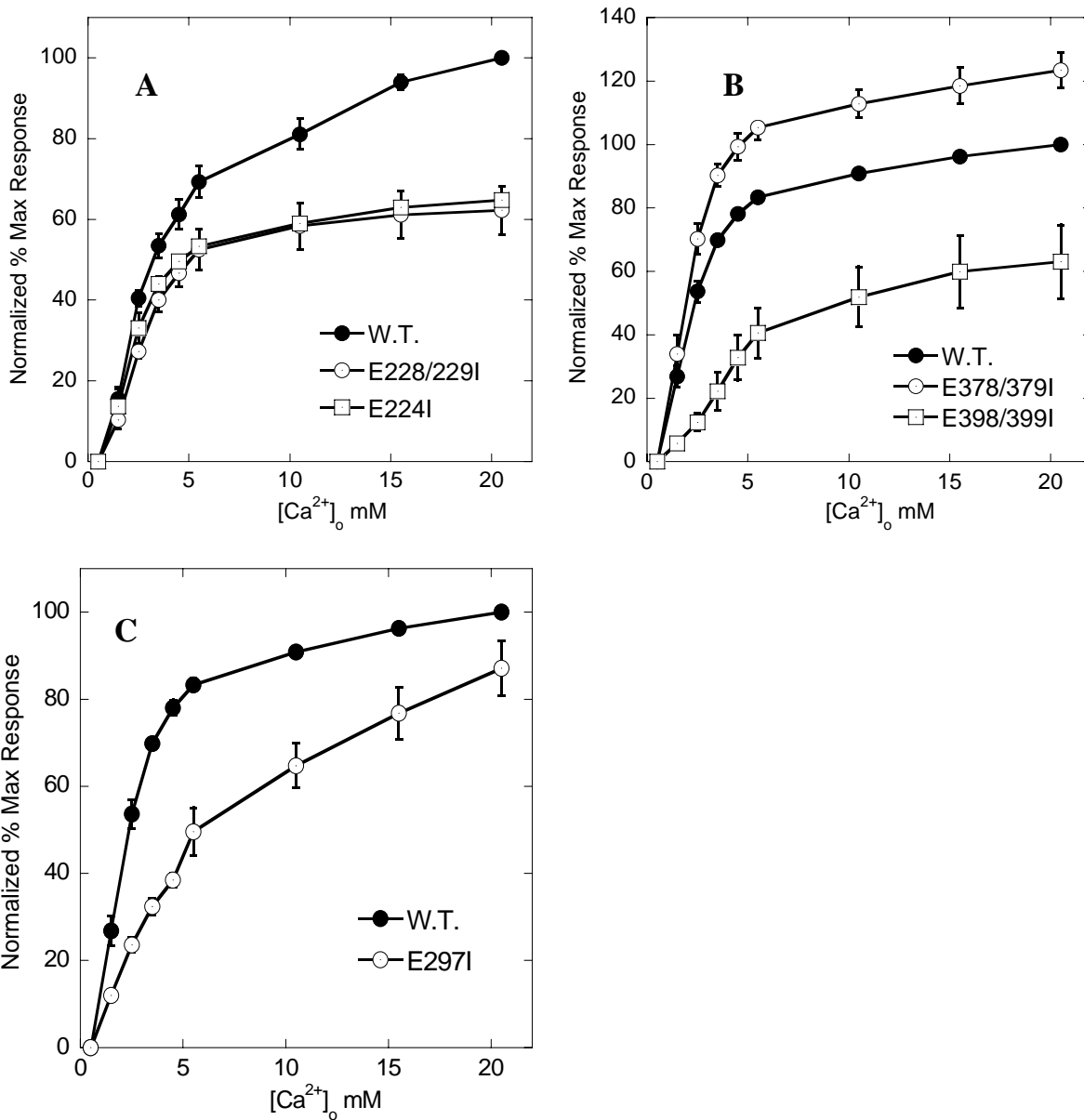


Figure 3

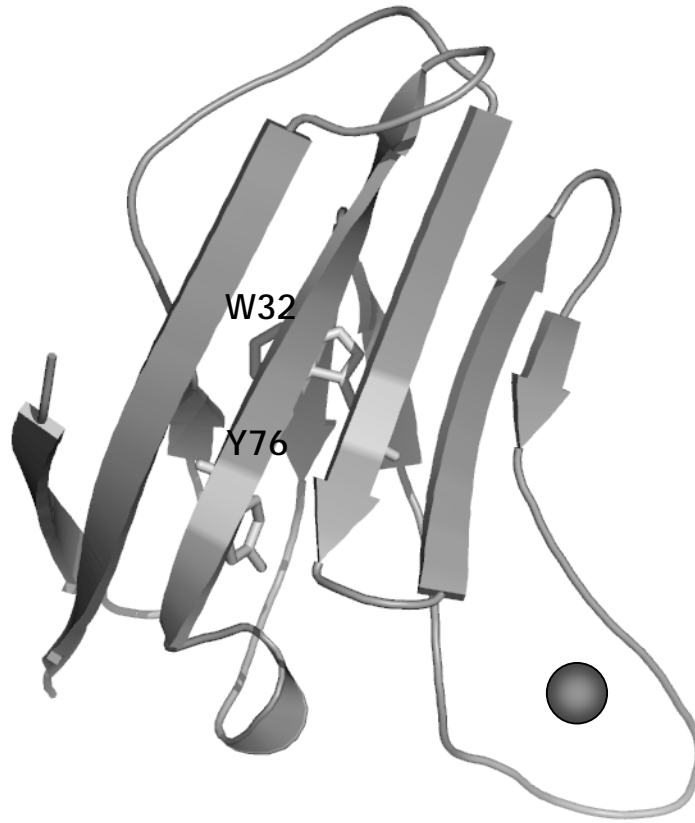


Figure 4

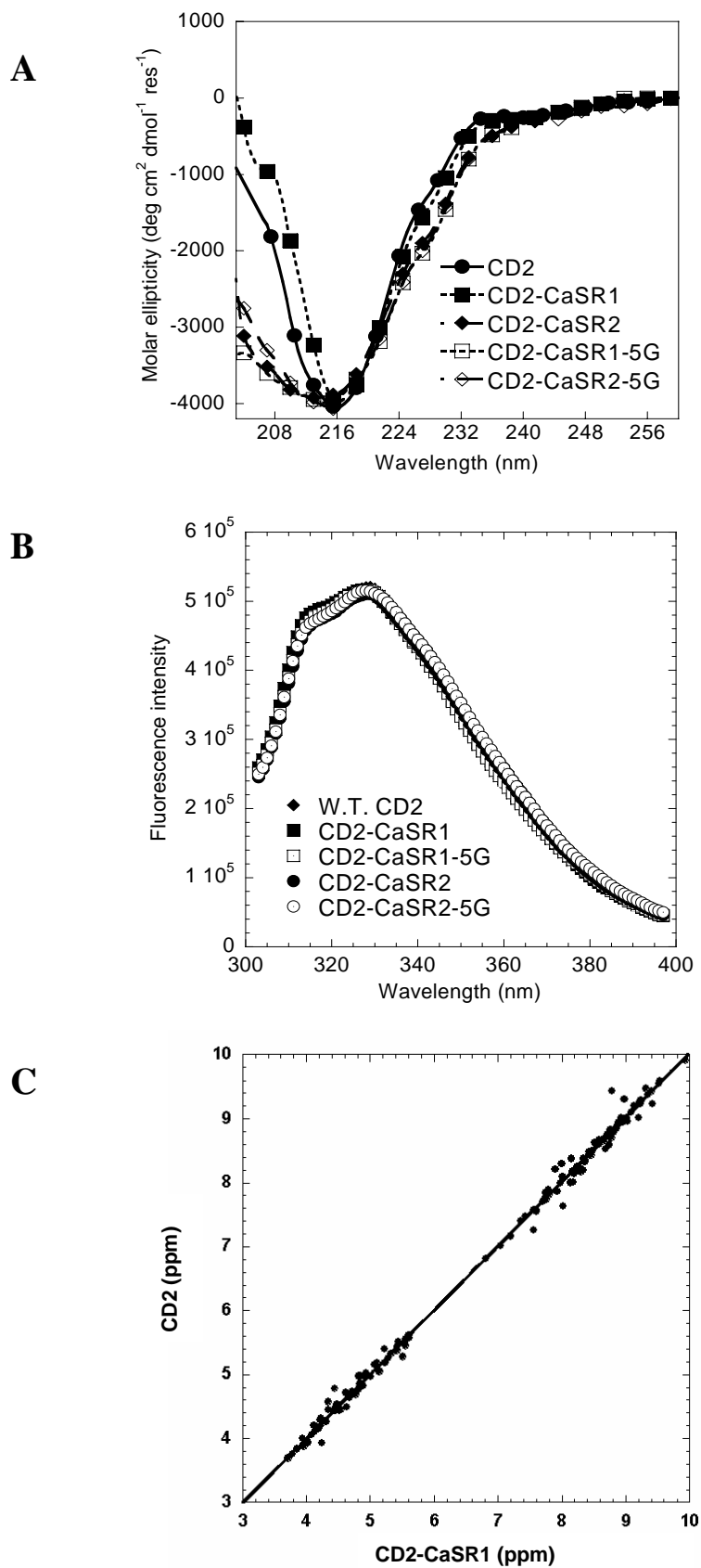


Figure 5 A-B

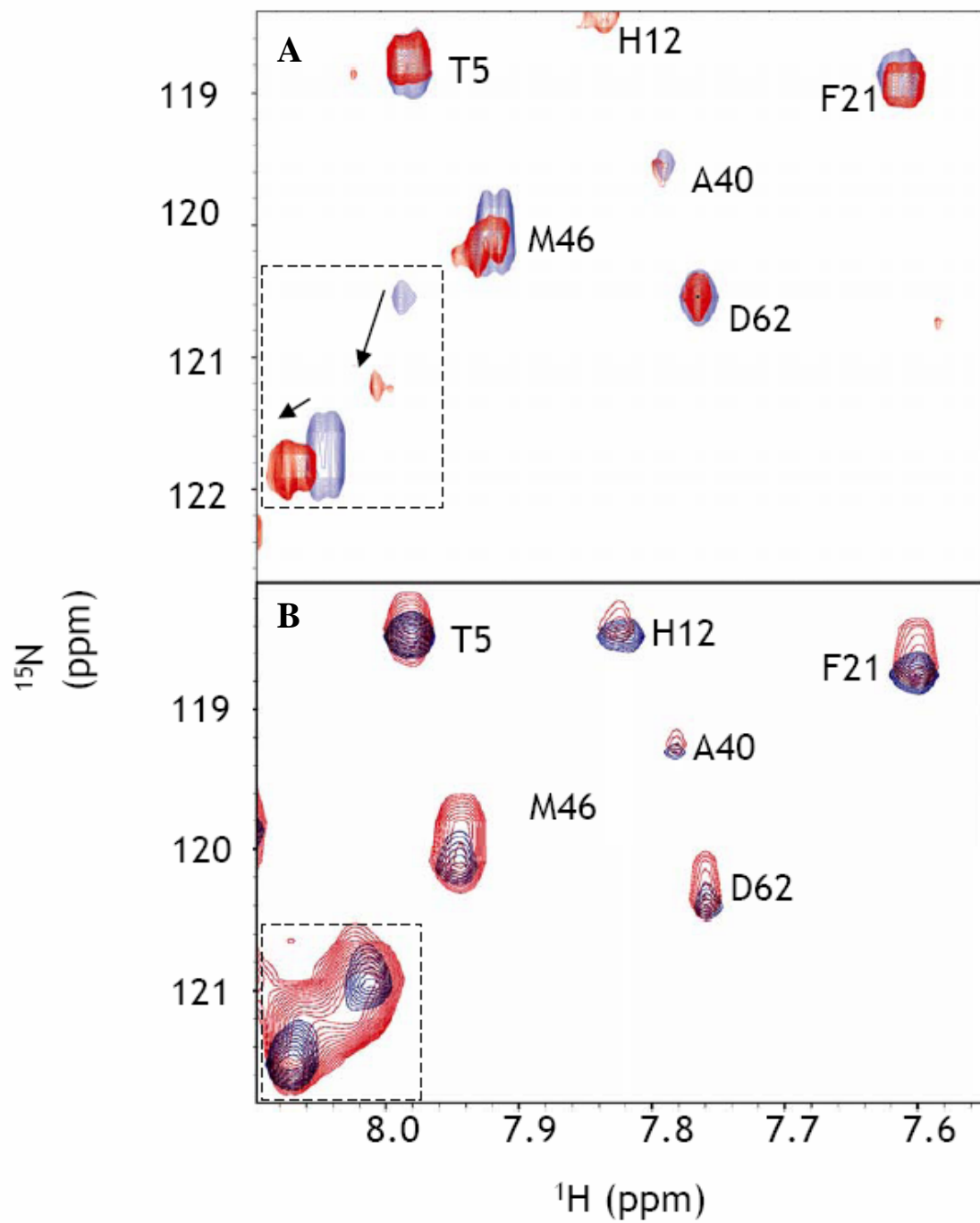


Figure 5 C-D

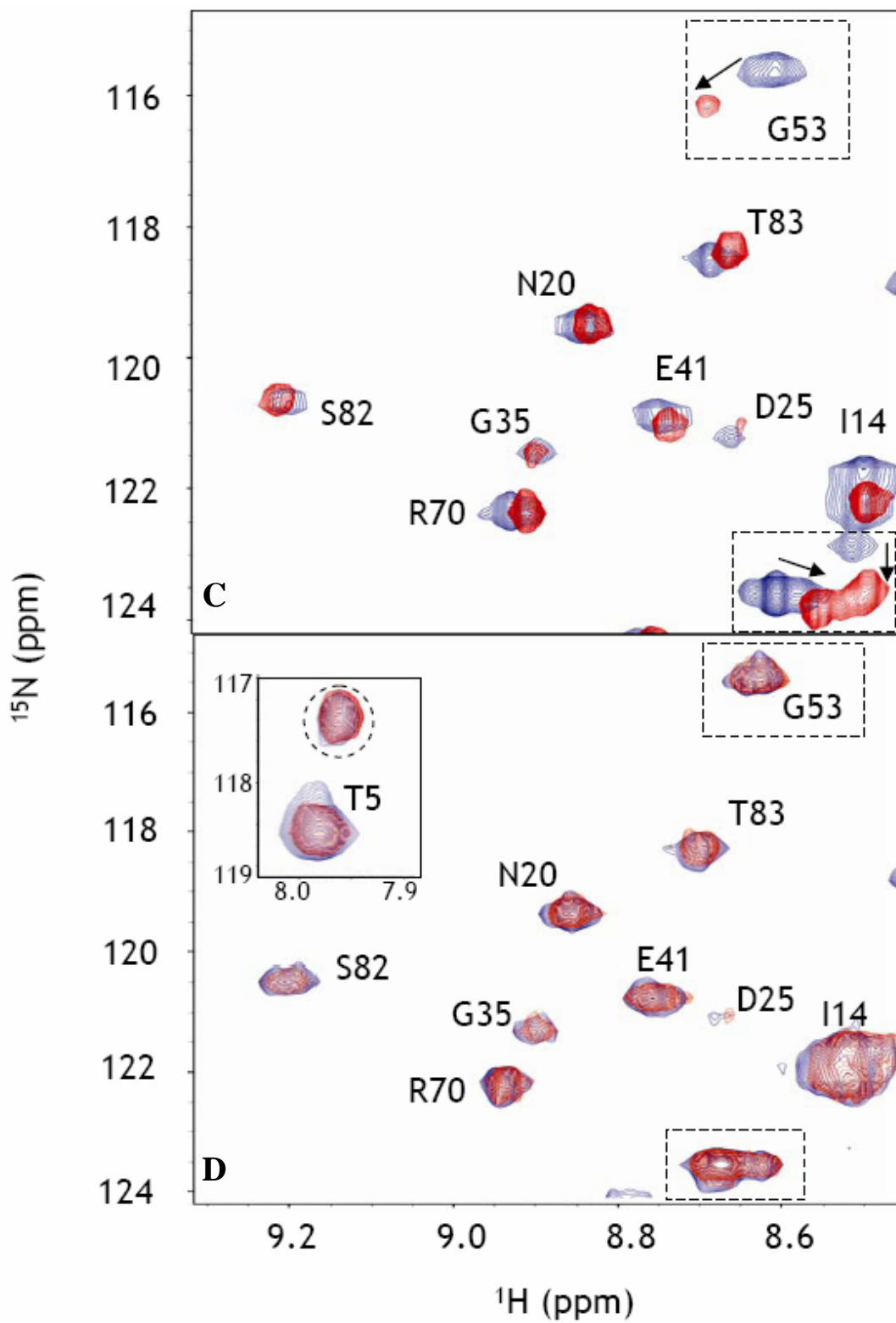


Figure 6

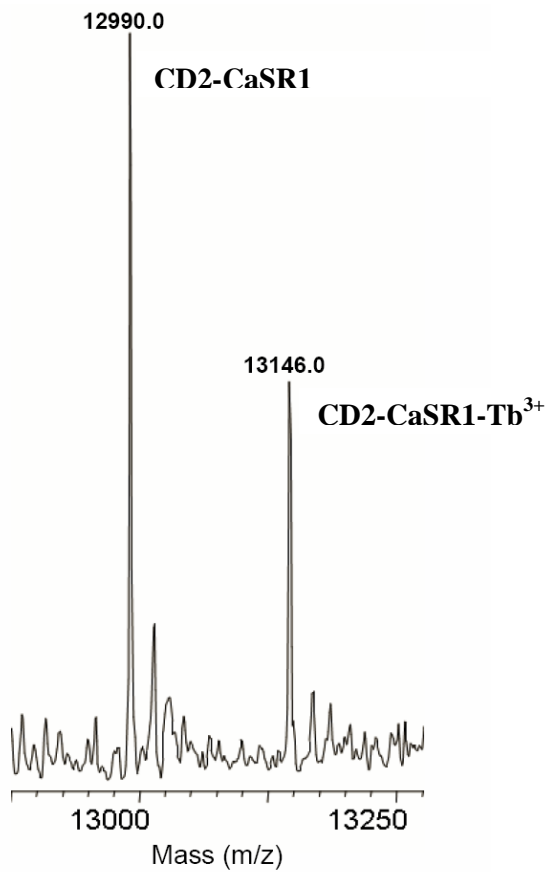
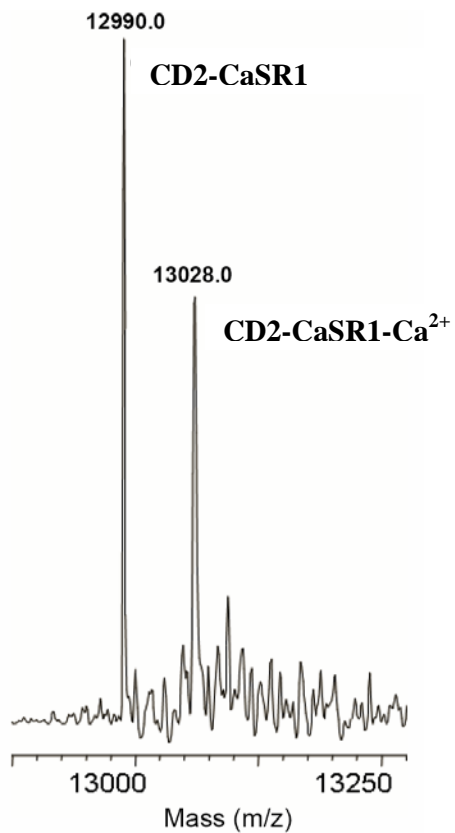


Figure 7

